Cell Host & Microbe
Article

Shigella Subverts the Host Recycling Compartment to Rupture Its Vacuole

Nora Mellouk,[1] Allon Weiner,[1] Nathalie Aulner,[2] Christine Schmitt,[2] Michael Elbaum,[3] Spencer L. Shorte,[2] Anne Danckaert,[2,*] and Jost Enninga[1,*]
[1]Institut Pasteur, Dynamics of Host-Pathogen interactions Unit, 25 Rue du Dr. Roux, 75724 Paris, France
[2]Institut Pasteur, Imagopole, 28 Rue du Dr. Roux, 75724 Paris, France
[3]Department of Materials and Interfaces, Weizmann Institute of Sciences, 234 Herzl Street, Rehovot 76100, Israel
*Correspondence: anne.danckaert@pasteur.fr (A.D.), jost.enninga@pasteur.fr (J.E.)
http://dx.doi.org/10.1016/j.chom.2014.09.005

SUMMARY

Shigella **enters epithlial cells via internalization into a vacuole. Subsequent vacuolar membrane rupture allows bacterial escape into the cytosol for replication and cell-to-cell spread. Bacterial effectors such as IpgD, a PI(4,5)P2 phosphatase that generates PI(5)P and alters host actin, facilitate this internalization. Here, we identify host proteins involved in *Shigella* uptake and vacuolar membrane rupture by high-content siRNA screening and subsequently focus on Rab11, a constituent of the recycling compartment. Rab11-positive vesicles are recruited to the invasion site before vacuolar rupture, and Rab11 knockdown dramatically decreases vacuolar membrane rupture. Additionally, Rab11 recruitment is absent and vacuolar rupture is delayed in the *ipgD* mutant that does not dephosphorylate PI(4,5)P_2 into PI(5)P. Ultrastructural analyses of Rab11-positive vesicles further reveal that *ipgD* mutant-containing vacuoles become confined in actin structures that likely contribute to delayed vacular rupture. These findings provide insight into the underlying molecular mechanism of vacuole progression and rupture during *Shigella* invasion.**

INTRODUCTION

Numerous bacterial pathogens have evolved strategies for host cell entry during infection for survival and proliferation. Upon internalization, they are all engulfed within a membrane-bound vacuole derived from the host cell plasma membrane. Then the invading pathogens modulate this compartment avoiding fusion with lysosomes to create a replicative niche. Alternatively, they damage and rupture the vacuole to access the nutrient-rich host cytoplasm (Ray et al., 2009). Vacuolar modulation by the internalized pathogens involves the host membrane trafficking machinery. These pathways are tightly regulated by small GTPases of the Rab family. Highly compartmentalized, Rab proteins determine intracellular transport and organelle identity. They function as molecular switches that alternate between the active GTP-bound form and the inactive GDP-bound form coordinated by specific GTPase-activating proteins (GAPs) and GTPase exchange factors (GEFs) (Stenmark, 2009). During endocytosis, Rab5 is localized at early endosomes (EEs) and regulates clathrin-coated vesicle (CCV) transport from the plasma membrane to the EEs as well as homotypic EEs fusion. EEA1 is the Rab5 effector that mediates tethering/docking of EEs. Then, cargos are either successively trafficked to Rab7-associated late endosomes and lysosomes for degradation, or transported back to the cell surface via different recycling routes. Rab4 mediates fast endocytic recycling directly from EEs to the plasma membrane, whereas Rab11 mediates slow recycling through the perinuclear endocytic recycling compartment (ERC) (Grant and Donaldson, 2009). Despite numerous downstream effectors known to interact with Rab11, like Rab11-family interacting proteins (FIPs), actin, and microtubule motors, only three Rab11-GAPs named, Evi5, TBC1D11, and TBC1D15, and no human Rab11-GEFs have been identified to date (Welz et al., 2014).

Bacterial pathogens translocate virulence factors into host cells where they interfere with host Rabs and perturb trafficking. For instance, SopE and SopB from *Salmonella typhimurium* act, respectively, as a Rab5-specific GEF mimic and an inositol phosphatase. Both bacterial effectors have been implicated in the recruitment of Rab5 to the *Salmonella*-containing vacuole (SCV) promoting fusion with EEs, which is crucial for vacuolar maturation (Mallo et al., 2008; Mukherjee et al., 2001). Interestingly, *Legionella pneumophila* secretes both a GEF and a GAP, named DrrA and LepB, that induce a feedback activation loop of Rab1 to promote efficient fusion of endoplasmic reticulum-derived vesicles with the *Legionella*-containing vacuole (LCV) (Ingmundson et al., 2007). Although the interplay between membrane trafficking and bacterial pathogens contained within vacuoles has been extensively studied, their implication in host membrane rupture events remain largely unknown (Brumell and Scidmore, 2007).

Shigella flexneri (*Shigella*) is a Gram-negative bacterium responsible for bacillary dysentery in humans. Upon epithelial cell contact, *Shigella* promotes massive actin and plasma membrane rearrangements leading to its internalization within a vacuole. Then, *Shigella* rapidly escapes from this vacuole, replicates within the cytosol, and moves intra- and intercellularly (Ray et al., 2009). Importantly, *Shigella* injects a set of bacterial effectors through the mxi-spa type 3 secretion system (T3SS) that subvert host cell function during bacterial internalization. For instance, IpaC initiates actin polymerization at the invasion site in a Cdc42-dependent manner. In addition, it recruits and activates the tyrosine kinase c-src, further promoting actin polymerization (Mounier et al., 2009). Besides, *Shigella* also targets membrane

phospholipids via the effector IpgD, a PI(4,5)P_2 phosphatase that generates PI(5)P at the bacterial entry site. In epithelial cells, the depletion of PI(4,5)P_2 contributes to the actin dynamics notably by disrupting the connections between cortical actin and the plasma membrane, whereas the production of PI(5)P induces activation of the PI3-kinase/Akt pathway, thereby promoting host cell survival (Niebuhr et al., 2002; Pendaries et al., 2006; Ramel et al., 2011). Recent studies indicate that IpgD prevents T cell migration at the site of infection and blocks ATP release to attenuate inflammation, suggesting that it plays a role in evading the immune response (Konradt et al., 2011; Puhar et al., 2013).

Whereas the entry process into epithelial cells is rather well established, the molecular mechanism of vacuolar rupture used by *Shigella* remains to be defined. The T3SS effector/translocator proteins IpaB and IpaC have been shown to disrupt lipid vesicles in vitro and are required for contact-mediated hemolysis by *Shigella*, indicating their potential role in membrane disruption (Blocker et al., 1999; van der Goot et al., 2004). Furthermore, in macrophages, IpaB has been implicated in phagosomal escape and successive induction of cell death (High et al., 1992). Recent evidences suggest that IpaB can assemble into multiprotein complex structures within membranes to allow ion fluxes, leading to macrophages pyroptosis (Dickenson et al., 2013; Senerovic et al., 2012). Nevertheless, due to the absolute requirement of IpaB/IpaC to deliver bacterial effectors into the host cells, it is challenging to assess their direct contribution in vacuolar rupture. In this study, we used a combination of high-content and live-imaging approaches to identify components of the recycling compartment as targets of the *Shigella* effector IpgD required for efficient rupture of the *Shigella*-containing vacuole.

RESULTS

Identification of Host Factors Controlling the Successive Entry Steps of *Shigella* into Epithelial Host Cells

In order to identify host factors involved in the early steps of *Shigella* invasion of epithelial cells, we carried out a high-content siRNA library screen targeting genes with established roles in membrane trafficking. *Shigella* internalization was followed by the actin rearrangements at the entry site, and the successive step of vacuolar rupture was imaged using a sensitive FRET-reporter assay that takes advantage of the cleavable cephalosporin-derived substrate CCF4 localized in the host cytoplasm and bacteria expressing β-lactamase at their surface. Only upon vacuolar rupture, the FRET-reporter is hydrolyzed by β-lactamase, leading to a robust switch of fluorescence emission from green to blue (Ray et al., 2010). We combined the fluorescence readouts for bacterial entry and for vacuolar rupture in our screen establishing automated image analysis algorithm for simultaneous robust quantification of both steps. In brief, HeLa cells were transfected with the different siRNAs for 72 hr, loaded with the FRET-reporter, and then infected with wild-type *Shigella* prepared as described before using a moi of 10 for 1 hr (Ray et al., 2010). Nuclei and actin filaments were stained, and images of about 8,000 cells per well were automatically acquired and analyzed (Figures 1A and 1B; see also Supplemental Experimental Procedures, available online, for details).

After data normalization based on the strictly standardized mean difference (SSMD) method, 32 siRNA targeted genes were identified as robust hits. Intriguingly, we only found gene knockdowns that decelerated vacuolar rupture. This may be attributed to its rapid pace in the controls taking place within 10 min after host cell entry. Identified genes included well-characterized host factors that drive actin polymerization during *Shigella* invasion, such as the Rho GTPase Cdc42, as well as six subunits of the Arp2/3 complex (Figures 1C and S1). We selected a subset of the identified genes for further validation and characterization based on their strong phenotype assessed by statistical analysis ($|SSMD| > 3$; see also Experimental Procedures and Figures S1A and S1B for details) as well as their biological relevance and the functional protein association network database STRING (http://string-db.org) (Figure 1D). The depletion efficiencies of these siRNA targets were verified by qRT-PCR (Figure S1C). A number of our selected hits included markers of early endocytic trafficking, such as Rab5 (A, B, and C isoforms), EEA1, and synaptojanins (SYNJ1 and SYNJ2). Surprisingly, our analysis also revealed a network of proteins involved in sorting and/or recycling pathways, such as Rab4A, sorting nexins (SNX1 and SNX2), Rab11A, and VAMP2 (Figure 1D). Collectively, our screen results suggest a key role of endocytic and recycling pathways in the early step of *Shigella* invasion into epithelial cells leading to vacuolar rupture.

A Specific Subset of Rab-GTPase Family Members Is Recruited to the *Shigella* Entry Site

Little is known about host membrane trafficking during the early steps of *Shigella* invasion; hence we characterized the Rab-associated hits in more detail. We used Rab4-, Rab5-, and Rab11-EGFP chimeras together with mOrange-tagged actin to monitor their localization during *Shigella* invasion into epithelial cells by live confocal microscopy. Strikingly, Rab11 massively accumulated at the entry site of *Shigella* (Movie S1, left panel; Figure 2A). Besides, Rab5 was transiently recruited with Rab5-positive vesicles appearing and disappearing at the entry site in a highly dynamic manner (Movie S1, middle panel; Figure 2B). On the other hand, Rab4 was not enriched (Movie S1, right panel; Figure 2C). Furthermore, immunofluorescent staining of endogenous Rab5 and Rab11 confirmed their accumulation at the invasion site of *Shigella* within epithelial cells (Figure S2).

To characterize the dynamics of actin and Rabs quantitatively, we performed image analysis of our time-lapse data of host factor recruitment to the bacterial entry site (see Experimental Procedures). In brief, the fluorescence intensities in the 561 and 488 nm channels corresponding to actin-mOrange and Rab4-, Rab5-, or Rab11-EGFP signals were measured around invading *Shigella* for at least 40 entry foci per experimental condition. After data normalization and alignment with the time of actin focus appearance, the host factor recruitment was plotted over the measured time period. For example, actin foci formation shown in Figure 2D could be decomposed in three phases, consistent with the published literature (Ehsani et al., 2012). Upon bacterial contact, a dramatic increase in actin signal appeared within 5 min, and it remained present for the subsequent 5 min. Then, it slowly declined to its initial level within approximately 20 min. Interestingly, the quantitative analysis in Figures 2E and S2C showed a sharp increase in the Rab11-EGFP fluorescence intensity level very shortly (90 s) after the onset of actin foci formation,

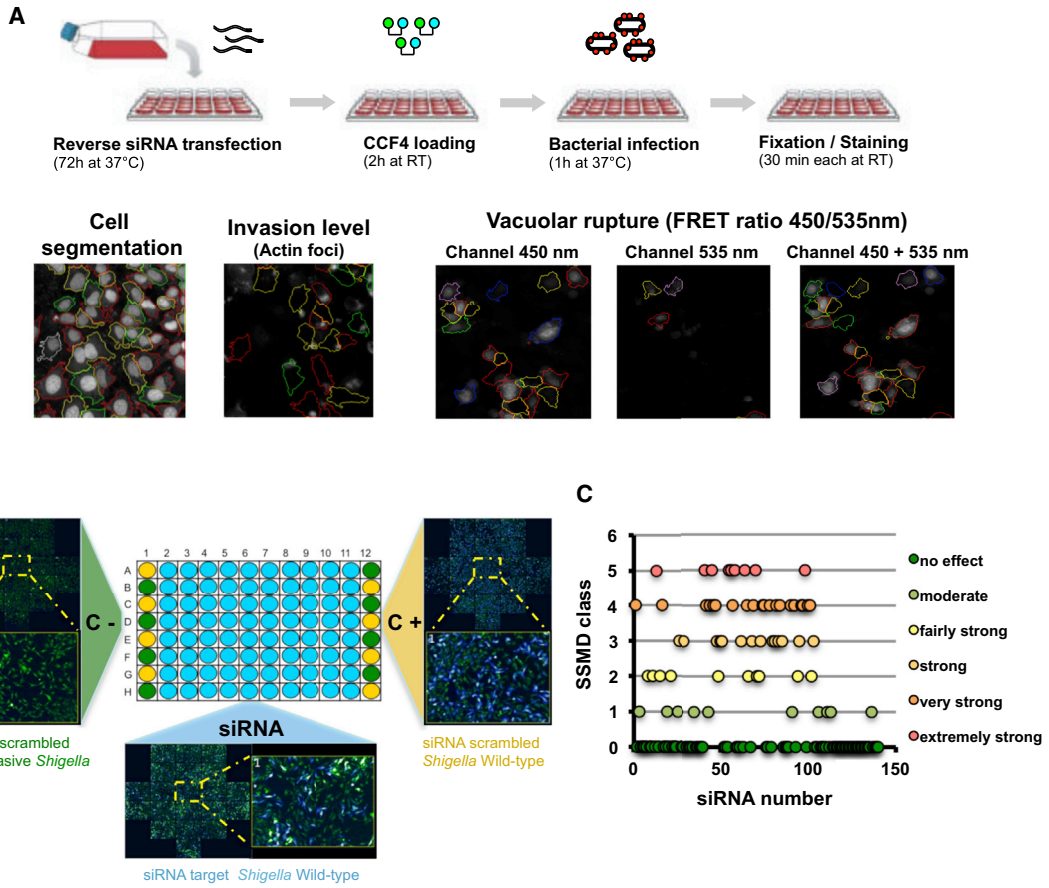

D

Gene	Description / Function	SSMD class
ARPC3	ARP2/3 complex. Actin polymerization.	5
Cdc42	Rho-GTPase. Actin polymerization.	5
EEA1	Tethering factor. Endocytosis.	5
Rab11A	Rab-GTPase. Slow endocytic recycling.	4
Rab4A	Rab-GTPase. Fast endocytic recycling.	4
Rab5A	Rab-GTPase. Endocytosis.	4
SNX1	Sorting nexin. Cargo sorting.	5
SYNJ2	Inositol phosphatase. Endocytosis.	4
VAMP2	SNARE. Docking and/or membrane fusion.	4

Figure 1. siRNA Screen Reveals Host Factors Required for Successive Steps of *Shigella* Invasion into Epithelial Cells

(A) Experimental pipeline. Host cells are grown in 96-well plates and transfected by siRNAs targeting proteins involved in membrane trafficking. Then they are loaded with the CCF4-AM FRET substrate to assess vacuolar rupture before challenging them with *Shigella*. After staining the nuclei and actin filaments, images are automatically acquired and analyzed. Cells are segmented, and *Shigella* entry is measured by actin foci formation and vacuolar rupture using the FRET ratio of CCF4.
(B) Screen layout. Representative 96-well plate showing the plate layout and images of the controls and a siRNA. Twenty images were acquired per well totaling about 64,000 cells per control condition and 32,000 cells per siRNA target.
(C) Overview of the screen results. Normalized SSMD values are plotted for each siRNA of the library identifying 32 siRNA targets as robust hit.
(D) Selected hit list of the screen. Among the hit list, nine host factors including members of the Arp2/3 complex and the Rab-GTPase family were selected for further validation and characterization.

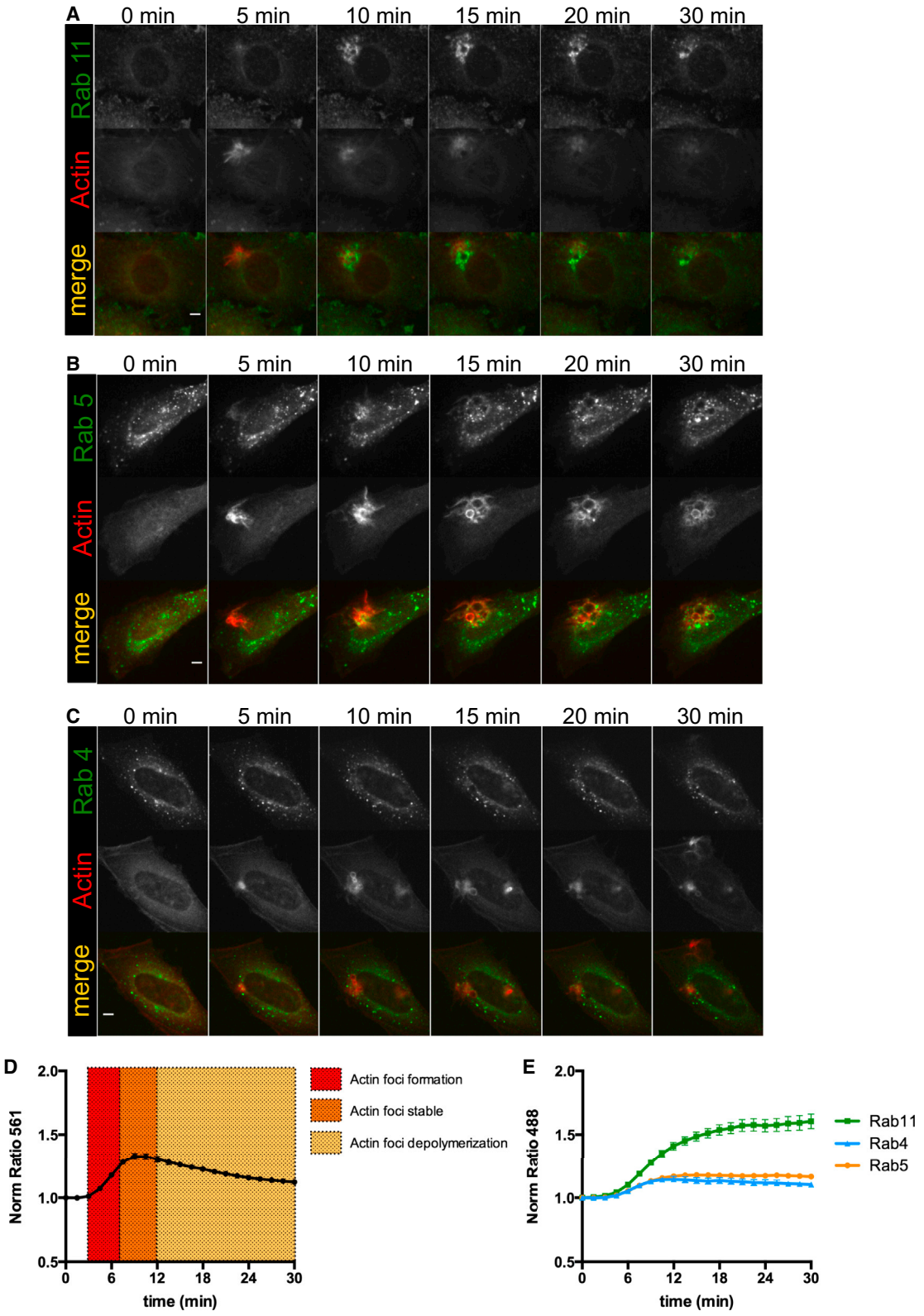

Figure 2. Recruitment of Rab-GTPase Family Members to the *Shigella* Entry Site

(A–C) Live confocal microscopy to monitor Rab localization during *Shigella* invasion into epithelial cells. HeLa cells expressing Rab4-, Rab5-, or Rab11-EGFP chimeras and actin-mOrange were infected with the *Shigella* WT and imaged. Rab11 massively accumulates, whereas Rab5 is transiently recruited at the entry foci of *Shigella* (A and B, respectively). In contrast, Rab4 is not specifically enriched at the *Shigella* invasion site (C). Scale bar, 5 μm.

(legend continued on next page)

and reaching an intensity plateau within approximately 10 min. Rab11 levels remained at high levels until the end of the measured time courses. Besides quantifying both Rab4 and Rab5-EGFP fluorescence intensity levels, we found them only slightly enriched (after about 6 min) remaining at fairly low levels throughout the measurement periods. Thus, our data revealed the massive recruitment of Rab11-positive vesicles and the transitory presence of Rab5-positive EEs at the vicinity of invading *Shigella* within epithelial cells, whereas Rab4-positive vesicles were not significantly enriched.

Rab11-Positive Vesicles Are Targeted by *Shigella* to Achieve Efficient Vacuolar Rupture

To correlate precisely the dynamics of Rab11 recruitment with the progression of *Shigella* invasion, we used the Galectin-3 marker to track vacuolar rupture (Paz et al., 2010). Time lapses of living cells cotransfected with Rab11-EGFP and Galectin-3-mOrange showed that Rab11 accumulation at the *Shigella* entry site took place before vacuolar escape (Movie S2; Figure 3A). In agreement with previously reported data, Galectin-3 was transiently recruited to the damaged membrane of the *Shigella*-containing vacuoles approximately 8 min after the beginning of the actin foci formation (Paz et al., 2010; Ray et al., 2010). Rab11 recruitment nearly reached its maximum before the bacteria ruptured their vacuoles (Figure 3B).

Then, we investigated in more detail the involvement of Rab11 during *Shigella* invasion. First, we performed gentamicin protection assays. As expected, the depletion of Cdc42 dramatically reduced *Shigella* internalization. In contrast, Rab11 knockdown did not alter the rate of bacterial entry (Figure 3C). Therefore, we next analyzed the successive steps of bacterial internalization and vacuolar lysis in living cells depleted for either Cdc42 or Rab11 by simultaneously tracking the onset of actin foci formation and the subsequent recruitment of Galectin-3. Knockdown efficiencies were measured by qRT-PCR at approximately 80% for Cdc42 and 95% for Rab11A (Figure S1). Confirming the gentamicin protection assay results, Rab11 knockdown did not affect the course of actin foci formation. Besides, Cdc42 knockdown did not completely inhibit but instead significantly delayed actin foci formation (Figure 3D). Nevertheless, once internalized into Cdc42-depleted cells, the bacteria ruptured their vacuoles similarly to the control condition (siRNA neg). In contrast, vacuolar rupture was strongly delayed in Rab11-depleted cells, arguing that *Shigella* recruits Rab11-positive vesicles to achieve efficient disruption of its vacuole (Figure 3E). This is further supported by the fact that a substantially lower number of bacteria are moving intracellularly by forming an actin tail when Rab11 is knocked down (Figure S3).

The Bacterial Inositol Phosphatase IpgD Is Required for the Recruitment of Rab11 Vesicles to the *Shigella*-Containing Vacuoles

Given our findings, we hypothesized that *Shigella* subverts Rab11 by the injection of T3SS effectors. Because phosphoinositides (PIs) are important in vesicular trafficking, we targeted the IpgD effector, a bacterial phosphatidylinositol 4-phosphatase (Niebuhr et al., 2002). First, the dynamic accumulation of Rab11 at the bacterial entry site was followed by live confocal microscopy in HeLa cells infected either with the *Shigella ipgD* strain, the *ipgD*/IpgD complemented strain, or the *ipgD*/IpgD^{C438S} strain complemented with a phosphatase-inactive mutant of IpgD (IpgD^{C438S}). Unlike for *Shigella* WT, Rab11 was not recruited at the entry site of both the *ipgD* and *ipgD*/IpgD^{C438S} strains (Movie S3, left panel and right panel; Figures 4A and 4C). Importantly, Rab11 recruitment was restored at the invasion site upon complementation in *trans* (Movie S3; Figure 4B). Indeed, quantitative analysis as in Figure 2D demonstrated that the differences between *Shigella* WT and the *ipgD* strains lacking the inositol phosphatase activity were highly significant ($p < 0.0001$). On the other hand, the recruitment of Rab11 by the *ipgD*/IpgD strain was similar to *Shigella* WT during the entire time course of infection. Albeit, a slight decrease of signal was observed toward the end of the measured time courses, likely due to a complementation effect (Figures 4D and S4). Therefore, the recruitment of Rab11-positive vesicles at the invasion site of *Shigella* requires the PI phosphatase activity of IpgD. Next, we investigated the role of IpgD in the remodeling of PIs at the invasion site of *Shigella*. For this purpose, we used the fluorescent probes PI(4,5)P_2 PH-PLCδ and PI(3)P 2X-FYVE and antibodies against PI(4,5)P_2 and PI(4)P (Figure S5; also see Supplemental Experimental Procedures for details). We found that PI(4,5)P_2 was depleted from the host cell plasma membrane in an IpgD-dependent fashion before the recruitment of Rab11-positive vesicles (Figures S5A–S5D), whereas its precursor PI(4)P was markedly enriched at the membrane ruffles independently of IpgD (Figure S5E). Additionally, we found the PI(5)P 3X-PHD(ING2) probe enriched at the invasion site of *Shigella* WT, but not at the vacuolar membrane, as described previously (Pendaries et al., 2006; data not shown). In contrast, PI(3)P was not detected at the membrane ruffles, nor around the nascent *Shigella*-containing vacuole. Nevertheless, a number of PI(3)P-positive large vesicles were dynamically located at the invasion site of *Shigella* WT but not *ipgD*, resembling their presence at macropinosomes (Figures S5F–S5H).

Correlative Large-Volume Microscopy Reveals Rab11-Positive Vesicles in the Vicinity of *Shigella* WT-Containing Vacuoles

To characterize structural details of the vesicles recruitment to the *Shigella* invasion site, we used a correlative light and electron microscopy (CLEM) approach. Because bacterial invasion takes place in three dimensions, we applied state-of-the-art large volume microscopy via focused ion beam/scanning electron microscopy (FIB/SEM) correlated with fluorescence light microscopy to obtain 3D-ultrastructural details of the invasion site of *Shigella* WT and *ipgD* within epithelial cells (Weiner et al., 2011). The same positions of interest were identified at both microscopes using MatTek dishes with a finder grid (Figure S6). After

(D and E) Quantitative analysis of the live-imaging data. The mean normalized fluorescence intensities in the 561 nm channel (Norm Ratio 561) and 488 nm channel (Norm Ratio 488) corresponding to actin-mOrange and Rab4-, Rab5-, or Rab11-EGFP signals confined to the invasion site of *Shigella* WT were assessed. For each entry event, the Rab intensity signals were aligned using the time point of the actin focus formation onset. Plotted are mean data ± SEM from at least three independent experiments ($n \geq 40$ per condition).

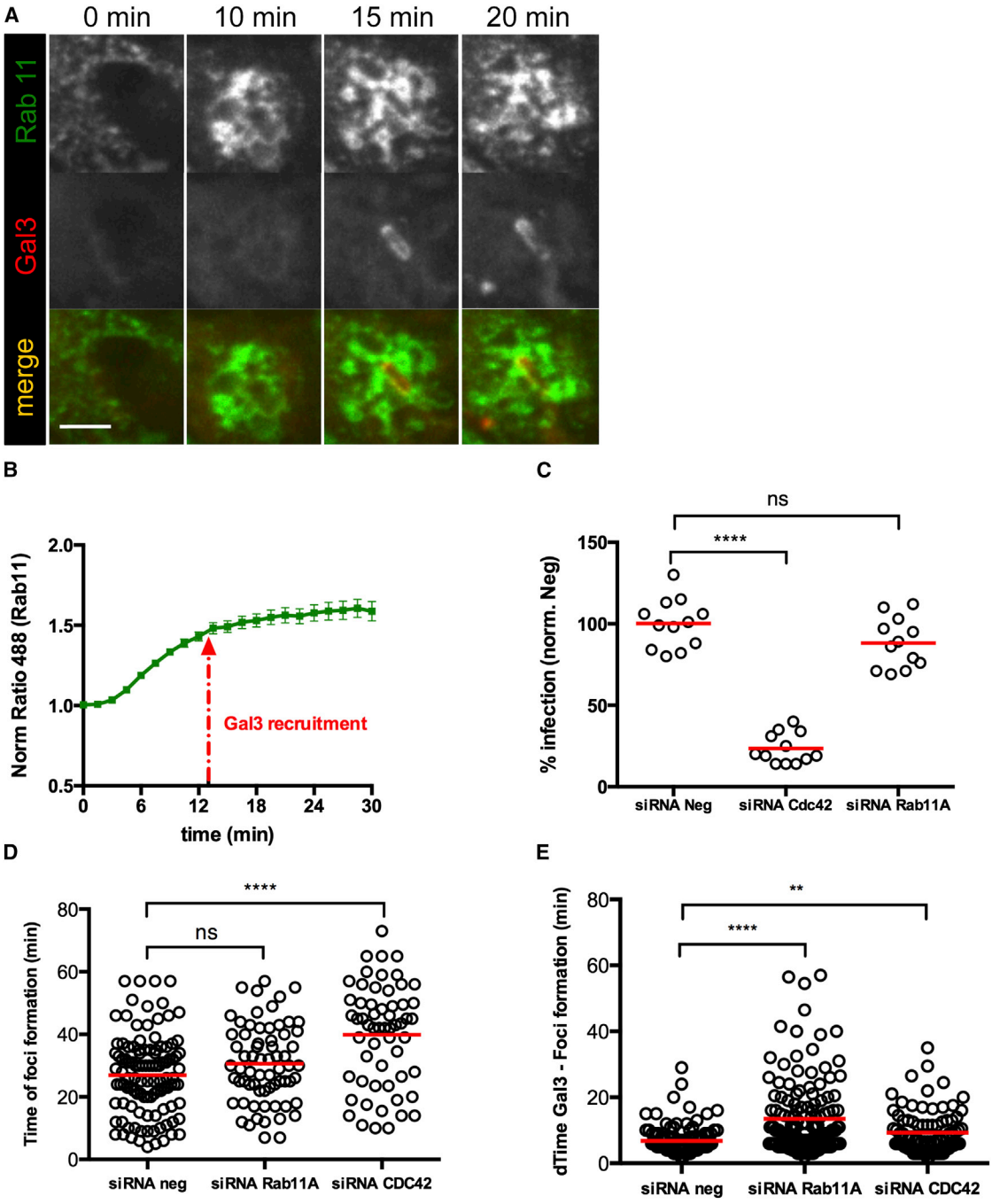

Figure 3. Rab11 Knockdown Impairs Efficient Rupture of *Shigella*-Containing Vacuoles

(A and B) Rab11 accumulation at the *Shigella* entry site takes place before vacuolar escape. (A) HeLa cells cotransfected with Rab11-EGFP and Galectin-3-mOrange were infected with the *Shigella* WT and imaged. Scale bar, 5 μm. (B) Quantitative analysis of Rab11 recruitment to the *Shigella* entry site during invasion. The red arrow indicates the mean time of Galectin-3 recruitment highlighting vacuolar rupture after the time point of bacterial entry measured by the onset of actin foci formation (see Figure 2D).

(C) Rab11 knockdown does not alter *Shigella* internalization into epithelial cells. Gentamicin protection assays depict the invasion level of *Shigella* WT into HeLa cells after 72 hr of siRNA transfection. Results were obtained from three independent experiments (n = 4 per condition) and statistically analyzed using the Mann-Whitney test.

(D and E) Rab11 knockdown results in a strong delay in vacuolar rupture. HeLa cells were cotransfected with actin-mOrange and Galectin3-EGFP to simultaneously monitor the entry step of *Shigella* by determining the time of actin foci formation (D) and the vacuolar rupture step by measuring the time interval (DT) between entry foci formation and Galectin-3 recruitment (E). Results were obtained from three independent experiments ($n \geq 60$ per condition) and statistically analyzed using the t test for foci formation and the Mann-Whitney test for vacuolar rupture (ns, nonsignificant difference).

transfection with Rab11-EGFP, cells were infected with *Shigella* WT or *ipgD* strains for 30 min and fixed. DNA (host cell nuclei and bacteria) and actin filaments were stained, and infected cells were imaged by confocal microscopy followed by processing for EM (see Experimental Procedures for more details).

Representative fluorescence images of host cells infected with *Shigella* WT or *ipgD* are shown in the upper panels of Figures 5A and 5B, respectively. Both DAPI and Rab11 fluorescence signals were delineated by thresholding to further correlate them with the ultrastructural data sets (also see Figure S6). In the lower panels, FIB/SEM data of the same invasion sites are shown, including a segmentation of bacteria-containing vacuoles (in blue) and vesicles (in orange). The Rab11 fluorescence signal (in green) was superimposed on the FIB/SEM data to obtain the correlative analysis of the *Shigella* invasion sites. Strikingly, the *Shigella* WT-containing vacuoles were surrounded by a large number of heterogeneous vesicles, which partially colocalize with Rab11 fluorescence signal (Figure 5A; Movie S4, upper panel). By contrast, only very few vesicles were present around the *ipgD*-containing vacuoles, and none were Rab11 positive (Figure 5B; Movie S4, lower panel). Furthermore, some of the Rab11-positive vesicles observed appeared to be in contact with the bacterial-containing vacuole, perhaps in the process of fusion or fission (Figure 5A; Movie S4, upper panel). However, the precise nature of these contacts requires further investigation. Thus, our correlative large volume microscopy data revealed the presence of Rab11-positive vesicles in the vicinity of *Shigella* WT-containing vacuoles, which was dependent on the bacterial effector IpgD.

Shigella ipgD Vacuolar Rupture Is Strongly Delayed with Bacteria Trapped in "Actin-Cage" Structures Compared to *Shigella* WT

We compared the dynamics of *Shigella* WT and *ipgD* invasion by monitoring the actin and Galectin-3 signals in living cells similarly to the analysis of Rab11 knockdown (Figures 3D and 3E). Although the entry site of *ipgD* displayed an altered morphology compared to the WT, both strains entered epithelial cells at the same pace (Figures 6A and 6C; Movie S5 and Movie S6), confirming previously reported data (Niebuhr et al., 2002). By contrast, we found that *Shigella ipgD* vacuolar rupture was significantly delayed, doubling the time period required for Galectin-3 recruitment to the damaged vacuole in comparison to *Shigella* WT (Figure 6B; Movie S5 and Movie S6).

Additionally, a more detailed analysis of these time-lapse image series provided a precise description of the events surrounding vacuolar destabilization during invasion by the *Shigella* WT and *ipgD* strains (Figures 6C and 6D; Movie S5 and Movie S6). *Shigella* entry started while triggering an actin focus that is less pronounced for *ipgD*. Upon bacterial internalization, *Shigella* WT rapidly disrupted its vacuole highlighted by the recruitment of the host Galectin-3 strongly accumulating at the damaged vacuolar membrane, thereby forming readily visible "Galectin-3 ghosts." In contrast, *Shigella ipgD* remained confined in a structure that resembled an "actin cage" stabilizing vacuolar membrane integrity. In-depth controls were performed to confirm that the *ipgD* mutant surrounded by an actin cage are within a vacuole (Figure S7). It is noteworthy that 83% of the *ipgD*-containing vacuoles, but only 17% of the *Shigella* WT strain, were surrounded by an actin cage, potentially explaining the different kinetics of vacuolar rupture between the two strains. Eventually, we found that *ipgD* also destabilized its vacuole, yet less than 40% of vacuoles were surrounded by a complete "Galectin-3 ghost" similar to the one observed for the WT. In over 60% of the cases, the recruitment of Galectin-3 to the *ipgD*-containing vacuoles appeared incomplete. The final stage of *Shigella* invasion is the well-described formation of an actin tail at one pole of the bacterium (Ray et al., 2010). Interestingly, we found that only 34% of *ipgD* bacteria formed an actin tail, in contrast to 96% of *Shigella* WT reflecting the delay of vacuolar escape into the host cytosol (Figures 6C and 6D; Movie S5 and Movie S6). To further support this notion, infected cells harboring *Shigella ipgD*-actin cages were treated with latranculin A, a chemical inhibitor of actin polymerization, and followed by live confocal imaging. Remarkably, the actin cage disassembled upon treatment, rapidly followed by vacuolar rupture as assessed by the recruitment of a complete Galectin-3 ghost (Figure S7D). Overall, our time-lapse data revealed that *ipgD*-containing vacuoles are confined in an actin cage prior to vacuolar rupture that appears to protect it from the subsequent rupture process.

DISCUSSION

Using a high-content siRNA screening approach, we found that *Shigella* particularly targets Rab11, a component of the host recycling compartment, by injecting its T3SS effector IpgD to achieve efficient vacuolar escape. Such subversion of the host is intriguing because vacuolar rupture has been assumed to be controlled directly by bacterial factors. For example, the T3SS effector/translocators IpaB and IpaC have been implicated in membrane destabilization due to their ability to insert into the host cell membrane for the delivery of bacterial effectors (Dickenson et al., 2013; High et al., 1992; Senerovic et al., 2012). Nevertheless, T3SS translocators with high homology to IpaB/IpaC are also present in numerous vacuolar bound Gram-negative bacterial pathogens (e.g., *Salmonella*, *Yersinia*, *Pseudomonas*), arguing for the existence of additional factors or other mechanisms controlling vacuolar membrane integrity during *Shigella* infection (Coburn et al., 2007; Håkansson et al., 1996; Hume et al., 2003). Apart from Rab11, we also found other host proteins involved in the step of *Shigella* vacuolar rupture. This suggests a complex mechanism where several host pathways are hijacked by the pathogen that is also supported by the deceleration of vacuolar rupture, but not to a complete inhibition after Rab11 knockdown. Involvement of multiple proteins from the host protein machinery in vacuolar escape has also been proposed for *Listeria* via the γ-interferon inducible lysosomal thiol reductase (GILT), the cystic fibrosis transmembrane conductance regulator (CFTCR), and via the heat shock protein HSP70 (Davis et al., 2012; Radtke et al., 2011; Singh et al., 2008). In the case of *Francisella*, the v-ATPase or the ubiquitin ligase CDC27 has been connected with the rupture process (Akimana et al., 2010). Together, it emerges that host factors are common targets for bacterial vacuolar escape.

A widespread strategy used by intravacuolar pathogens is the subversion of host vesicular trafficking to avoid lysosomal degradation and subsequently promote bacterial proliferation (Brumell and Scidmore, 2007). Altering endocytic trafficking expressing

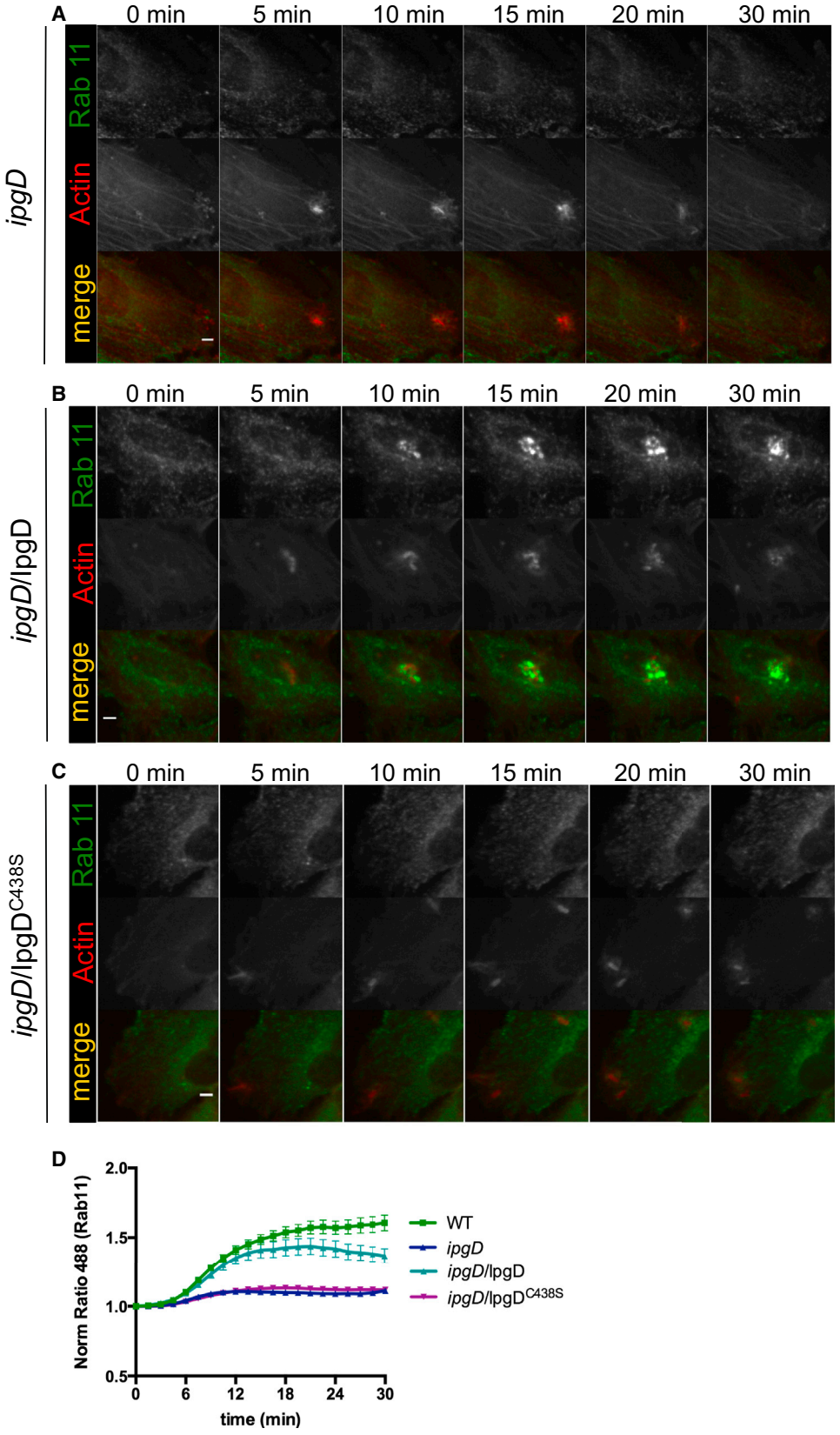

(legend on next page)

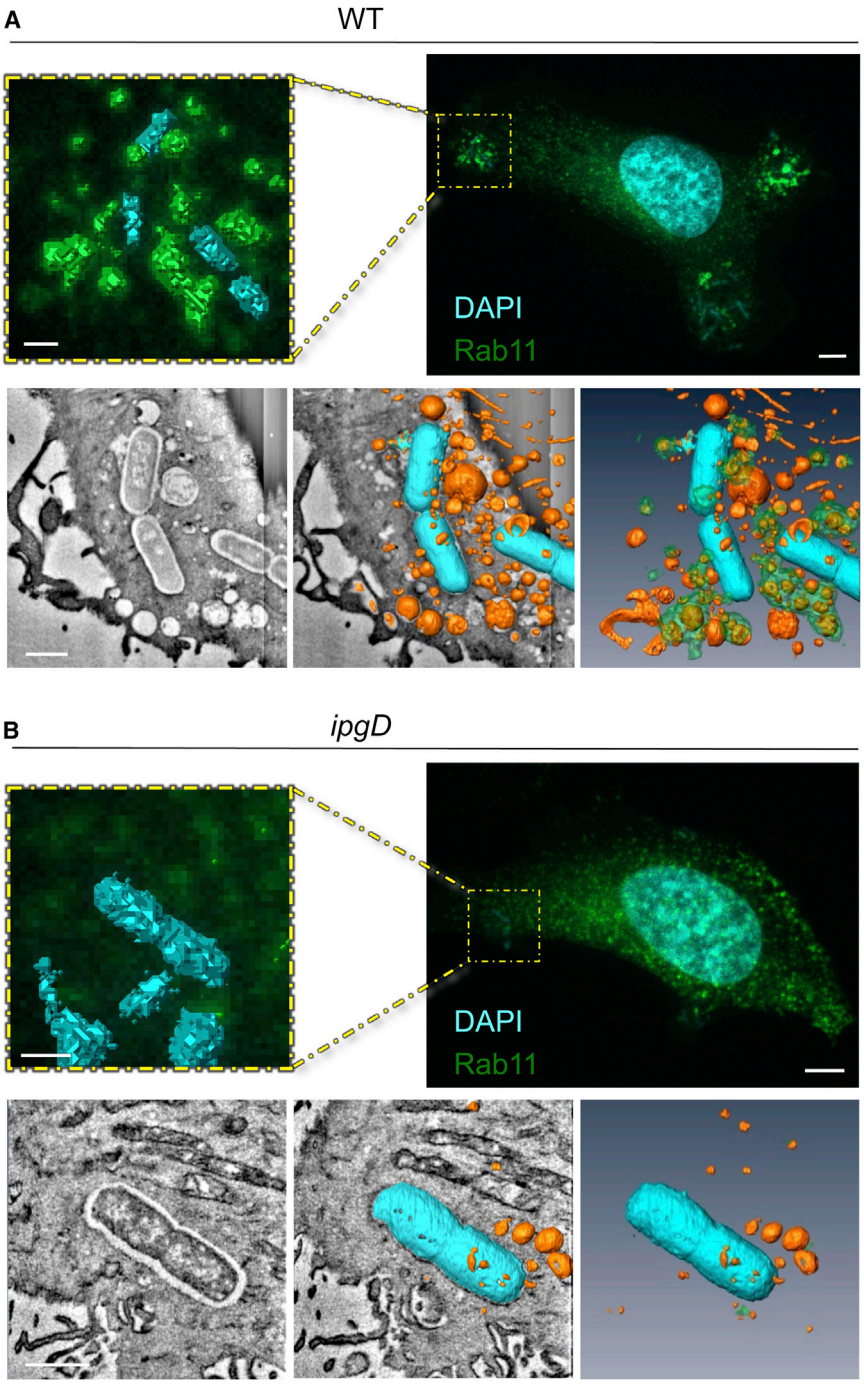

Figure 5. Ultrastructural Characterization of the *Shigella* WT and *ipgD* Invasion Site Using Large-Volume Correlative Microscopy

(A and B) Fluorescence confocal microscopy was followed by large volume FIB/SEM of the same invasion site of *Shigella* WT (A) or *ipgD* (B) within host epithelial cells. Image of the entire host cell with Rab11-EGFP and DAPI fluorescence signals is shown in upper right corner (scale bar, 5 μm). A zoom image of the invasion site including the segmentation of both Rab11-EGFP and DAPI fluorescence signals is shown in upper left corner (scale bar, 1 μm). FIB/SEM image of the same invasion site is shown in lower left corner (scale bar, 1 μm). Using Amira software, the bacteria-containing vacuoles and host vesicles were segmented from the 3D EM data set (shown in blue and orange, respectively). Fluorescent Rab11-positive vesicles (green) were correlated with the host vesicles (orange).

constitutively active Rab5 or dominant-negative Rab7 leads to vacuolar destabilization of SCVs (Brumell et al., 2002). Our study reveals the massive recruitment of Rab11-positive vesicles to the *Shigella*-containing vacuoles, whereas Rab5-positive EEs only transiently appear and disappear, and Rab4-positive vesicles are not enriched. Rab11 knockdown strongly delays the vacuolar rupture of *Shigella* without affecting the entry within epithelial cells. Interestingly, *Chlamydia* also recruits Rab11 to the inclusion, and both Rab11 and Rab6 knockdown prevent Golgi fragmentation, causing a defect in lipid transport to the inclusion and bacterial proliferation (Derré et al., 2007; Rejman Lipinski et al., 2009). Also, *Legionella* recruits Rab11 to its vacuole; however, this does not impair intracellular bacterial replication (Hoffmann et al., 2014). It would be interesting to address whether it has an impact on the vacuolar membrane integrity using fluorescent markers as in this work. Recently, Mounier et al. have shown that *Shigella* induces Golgi fragmentation via IpaB-dependent cholesterol relocalization. They described also the tubulation of transferrin (Tf)- and Rab11-positive compartments leading to an impairment of recycling after 45 min p.i., a time point when *Shigella* is already proliferating within the cytosol (Mounier et al., 2012). We found an early implication of Rab11 during *Shigella* invasion that occurs via

Figure 4. The Bacterial Inositol Phosphatase IpgD Controls the Recruitment of Rab11 to the *Shigella*-Containing Vacuoles

(A–C) Live confocal microscopy shows the requirement of the enzymatic action of IpgD to recruit Rab11 to invading *Shigella*. HeLa cells cotransfected with Rab11-EGFP and actin-mOrange were infected with a *Shigella ipgD* strain (A), a *ipgD*/IpgD strain complemented in *trans* (B), or *ipgD*/IpgD^{C438S} strain complemented with an inositol phosphatase inactive IpgD^{C438S} (C) and imaged. Rab11 was not recruited at the entry foci of both *Shigella ipgD* and *ipgD*/IpgD^{C438S} strains. However, it was restored at the invasion site of the *ipgD*/IpgD. Scale bar, 5 μm.

(D) Quantitative analysis of Rab11 recruitment at *Shigella* invasion site using different bacterial strains (see Figure 2E and Experimental Procedures). Mean data ± SEM from at least three independent experiments ($n \geq 30$ per condition) are plotted.

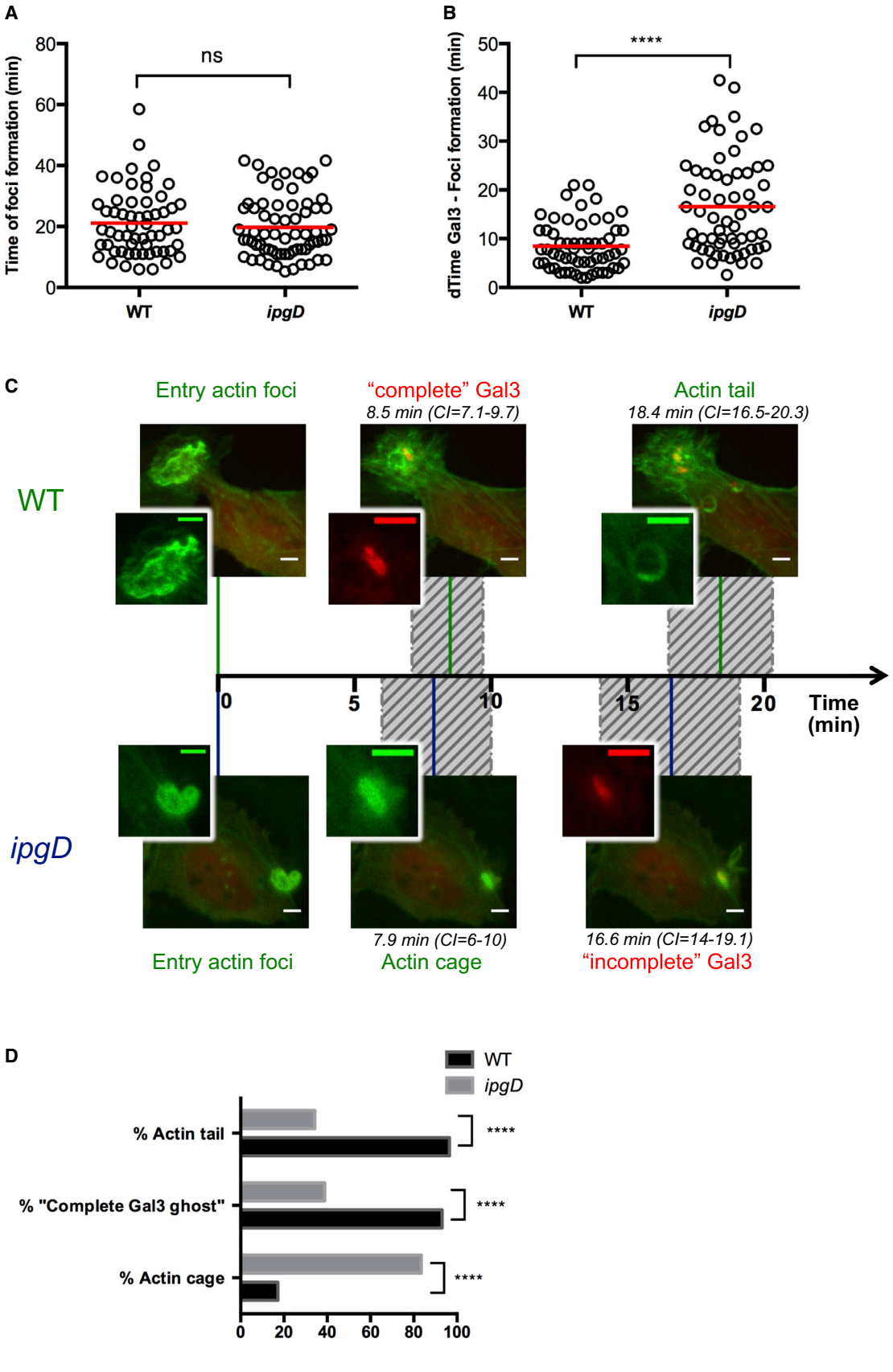

(legend on next page)

recruitment to the entry site within minutes and is surprisingly only accompanied by weak Tf colocalization (data not shown), suggesting that both processes are distinct. Indeed, similar tubulation is observed with VAMP4, a SNARE present at the trans-Golgi network, but not with VAMP3, which is a RE marker that also accumulates at the invasion site of *Shigella* (data not shown). Thus, the tubulation of Tf- and Rab11-positive compartments is probably due to the disruption of the retrograde pathway, whereas we report an involvement of the recycling pathway. This highlights the delicate subversion of distinct host pathways by *Shigella*. Interestingly, previously reported screen data suggest that Rab11 knockdown inhibits *Listeria* infection (Derré et al., 2007), raising the possibility that our findings can be extended to other cytosolic pathogens.

PIs are major spatiotemporal regulators of membrane trafficking, and numerous intracellular bacterial pathogens subvert PIs to ensure their survival and proliferation (Weber et al., 2009). In this regard, *Shigella* modulates PIs injecting the virulence factor IpgD, a $PI(4,5)P_2$ phosphatase producing PI(5)P (Niebuhr et al., 2002). Our results clearly show that the IpgD inositol phosphatase activity is required for the recruitment of Rab11-positive vesicles to the *Shigella*-containing vacuoles. In an attempt to determine how the remodeling of PIs by IpgD could promote Rab11 recruitment, we investigated the PIs pattern during *Shigella* invasion of host cells. Interestingly, we found that $PI(4,5)P_2$ is markedly depleted from the host cell plasma membrane at an early stage of the infection, before Rab11 recruitment occurs. This confirmed findings by Niebuhr et al. that assessed biochemically the cellular levels of PIs, notably revealing a global drop of $PI(4,5)P_2$ levels with a concomitant increase in PI(5)P controlled by the IpgD effector (Niebuhr et al., 2002). Nonetheless, none of the PI surveyed in this study (including $PI(4,5)P_2$, PI(5)P, PI(4)P, and PI(3)P) was found at the *Shigella*-containing vacuole. Collectively, our data suggest a mechanism of *Shigella* subverting its environment rather than the vacuolar membrane itself to lead to its rupture. It is noteworthy that PI(5)P has been shown to block the trafficking of activated EGFR on EEs, protecting it from lysosomal degradation, but spares the recycling and retrograde pathways (Ramel et al., 2011). In contrast, chemical inhibition of EGFR phosphorylation did not affect Rab11 recruitment induced by *Shigella* (data not shown). Thus, the accumulation of Rab11-positive vesicles at the invasion site of *Shigella* is not due to the recycling of activated EGFR, even though both are IpgD dependent.

Actin cages around *Listeria*- and *Shigella*-containing vacuoles have been reported previously by others and us (Ehsani et al., 2012; Yam and Theriot, 2004). However, actin cage dynamics around internalized bacteria as well as their role during bacterial invasion remain entirely unknown. Our data reveal that *ipgD*-containing vacuoles are more likely to be confined in actin cages than *Shigella* WT, suggesting a link with PIs. Furthermore, it is known that $PI(4,5)P_2$ regulates numerous actin-binding proteins promoting F-actin polymerization with local $PI(4,5)P_2$ enrichment and F-actin disassembly upon $PI(4,5)P_2$ hydrolysis (Janmey and Lindberg, 2004; Scott et al., 2005). Thus, it is tempting to propose that actin cage dynamics are tightly regulated by the $PI(4,5)P_2$ content at the *Shigella* invasion site. During cell division, Rab35 recruits the PI 5-phosphatase OCRL that depletes $PI(4,5)P_2$ to prevent F-actin accumulation at the intercellular bridge for successful abscission (Dambournet et al., 2011). Similarly, our data suggest that *Shigella* globally depletes $PI(4,5)P_2$ via IpgD, preventing the formation of a lasting actin cage around the bacteria-containing vacuole, thereby promoting vacuolar destabilization. Indeed, the actin cages could stabilize the bacteria-containing vacuoles by direct structural support. Likewise, *Salmonella*- and *Chlamydia*-containing vacuoles are surrounded by an F-actin meshwork resembling the actin cage structures in our study. Importantly, disruption of the actin mesh has also been correlated with vacuolar rupture for both of them (Kumar and Valdivia, 2008; Méresse et al., 2001). Alternatively, actin cages could indirectly affect vacuole stability by preventing the access or exchange with the host vesicular traffic. This is supported by our CLEM data on Rab11-positive vesicles at early stages of *Shigella* invasion with intact bacterial containing vacuoles. Furthermore, Rab11 knockdown does not affect vacuolar rupture through the formation of an actin cage. Taken together, this suggests that the fusion of Rab11-positive vesicles with the bacterial vacuole promotes its rupture.

Changes in the lipid and/or protein content of the membrane have mechanical and biochemical consequences that influence membrane stability. Interestingly, $PI(4,5)P_2$ hydrolysis has been shown to alter the membrane structure, notably due to the replacement of the large $PI(4,5)P_2$ polar headgroup by the small DAG headgroup (Hammond et al., 2006; Janmey and Kinnunen, 2006). Therefore, it is not surprising that modulation of lipid/protein composition of bacteria-containing vacuoles leads to strong phenotypes. For instance, the *Salmonella* effector SseJ depletes cholesterol from the SCV, thus increasing membrane fluidity and sensitivity to cytoskeleton motor-dependent forces, leading to a loss of vacuolar integrity (Ohlson et al., 2005).

Based on our findings, we propose a model for bacterial vacuolar rupture whereby the interaction with specific host vesicles by sequential fusion and fission events controls the fate of the bacteria-containing vacuoles, presumably by modulating the membrane composition and/or inducing physical stress.

Figure 6. The Bacterial Effector IpgD Is Required for Efficient Vacuolar Escape Induced by *Shigella* within Epithelial Cells

(A–D) Live confocal microscopy shows that *Shigella ipgD* entry into epithelial cells is not impaired but vacuolar rupture is strongly delayed compared to *Shigella* WT. HeLa cells cotransfected with pEGFP-actin and pOrange-Galectin were infected with *Shigella* WT or *ipgD*.

(A and B) Quantitative analysis of bacterial entry (time of actin foci formation onset) and vacuolar rupture (time interval (dTime) between entry foci formation and Galectin-3 recruitment) are plotted in (A) and (B), respectively. Results were obtained from three independent experiments (n = 60 per condition) and statistically analyzed using the Mann-Whitney test.

(C) Representation of the time course of the successive intracellular stage of *Shigella* WT and *ipgD* invasion into epithelial cells with representative images and the mean times with the 95% confidence intervals (CI) for each key step.

(D) Qualitative analysis of structural features during *Shigella* entry. Results were plotted as a percentage of total bacteria and statistically analyzed using the chi-square test.

EXPERIMENTAL PROCEDURES

Bacterial Strains, Cell Culture, and Infection

The bacterial strains, cell culture, and infection conditions used in this study are described in the Supplemental Experimental Procedures.

siRNA Library Screen

The Human Membrane Trafficking library of 140 siRNA SMARTpool from Dharmacon was tested in a medium-throughput siRNA screen. It consists of a pool of four different oligos for each target gene. Each 96-well plate (Greiner) of the screen was designed as follows: eight positive control wells, transfected with scrambled siRNA and challenged with invasive *Shigella* (M90T Afal); eight negative control wells, transfected with scrambled siRNA and challenged with noninvasive *Shigella* (BS176 Afal); and four replicates for each siRNA target, infected with the invasive *Shigella* (M90T Afal). Reverse siRNA transfection of HeLa cells was performed using the Lipofectamine RNAi max reagent (Life technologies) and a final siRNA concentration of 10 nM for 72 hr. Loading of cells with the CCF4/AM substrate (Life Technologies) was identical to previously established protocols (Ray et al., 2010). The siRNA library screen images were acquired on an automated confocal microscope OPERA QEHS (Perkin Elmer) with a 10× objective in the following sequence: CCF4 (ex/em 405/540 and 405/450 on two separated cameras), Rhodamine Phalloidin (ex/em 561/600), and Draq5 (ex/em 640/690) channels. Per well, a field of 20 adjacent images was acquired, covering ≈40%–50% of each measured 96-well plate. Automated image analysis was performed using a customized algorithm developed in the Acapella software (PerkinElmer). We used both the Z′ factor and the SSMD statistical tests for the scoring of our hits (see also Supplemental Experimental Procedures). The knockdown efficiencies of siRNA transfection were assessed by qRT-PCR.

Plasmids and Transfection

HeLa cells were seeded into 96-well plates at a density of 7,000 cells per well 24 hr prior to transfection. The cells were then transfected with one or two expression plasmids using X-tremeGENE 9 reagent (Roche) for 24 or 48 hr, according to the manufacturer's instructions. A list of the plasmids used in this study is provided in Table S1.

Time-Lapse Live-Cell Confocal Microscopy

Living cells were imaged at 37°C using a PerkinElmer UltraView spinning disc confocal microscope with a 40×/1.3 NA oil objective. Every 60 or 90 s, a stack of 13 z planes (step size of 500 nm) was acquired sequentially in two channels for 75 min using a 488 and 561 nm laser. Fluorescence emission was detected with 525 (W50) nm and 615 (W70) nm filters, respectively. After two time points, the image acquisition was paused to add the bacteria at a moi of 50.

Correlative Focused Ion Beam/Scanning Electron Large-Volume Tomography

We performed CLEM, using fluorescence confocal microscopy followed by FIB/SEM tomography. HeLa cells grown on Mattek dishes were fixed with 0.1% glutaraldehyde (GA) and 4% paraformaldehyde (PFA) for 30 min. After confocal microscopy imaging of the specimen details using a 60×/1.3 NA water objective, positions of interest were marked at 10× and 20× magnifications (Figure S6). After overnight fixation with 2.5% GA in 0.1 M cacodylate buffer, samples were treated with 2.5% GA supplemented with 0.4% tannic acid (pH 7.2) in 0.1 M cacodylate buffer for 30 min. Then they were stained with 1% OsO4 in DDW for 30 min at 4°C. Samples were then dehydrated and embedded in Epon. FIB/SEM large-volume tomography was performed in a Helios Nanolab Dual beam (FEI) as previously described (Weiner et al., 2011), except using the finder grid imprint in the resin to find sites of interest. Images were recorded with 0.69 nA or 1.4 nA at 2 kV in the immersion lens mode, with pixel sizes of 6.5 nm. For milling slices an ion beam current of 0.46 nA or 0.92 nA at 30 kV was used with a step size of 10 nm. Inverted contrast is presented. Amira (FEI) was used for correlating the light and electron microscopy data with internalized bacteria acting as aligning fiducials.

Image Analysis

Live-Cell Image Analysis of Shigella *Invasion*

All time-lapses shown are maximum 3D projections from entire z stacks assembled in ImageJ. Actin-mOrange and Galectin-3-EGFP image series were visually analyzed. *Shigella* entry was tracked determining the time points of the onset of actin foci formation. The successive step of vacuolar rupture was monitored measuring the time interval (DT) between the beginning of entry foci formation and the appearance of a Galectin-3 signal around the entering bacteria. Finally, bacterial intracellular motility was determined measuring the time interval (DT) between entry foci formation and actin comet tail formation.

Live-Cell Image Analysis—Quantification of Rab Recruitment at the Invasion Site

Using Volocity software (PerkinElmer), the fluorescence intensities in the emission channels at 488 and 561 nm (corresponding to the different Rab-EGFP fusions, and to Actin-mOrange) were measured within equally sized ROIs around the *Shigella* invasion sites, and plotted over time. For each curve, the maximum slope in the 561 nm channel was used to determine the time of actin focus appearance. Data were normalized by dividing the fluorescence intensity of each time point by the one at T0 (Norm Ratio 488), with T0 corresponding to the average value of the first three time points (4.5 min) before actin foci appearance.

Gentamicin Protection Assay

Gentamicin protection assays were performed as described before to assess the efficiency of *Shigella* invasion into epithelial cells (Mounier et al., 2009).

Statistical Analysis

Statistical analysis was performed in GraphPad Prism software v6. Differences between control and experimental groups were evaluated by two-tailed unpaired t tests, unless values were not normally distributed. In such cases the nonparametric Mann-Whitney test was applied. To compare two time course curves at each time point, the multiple t test method was used with correction using Holm-Šídák method (Aickin and Gensler, 1996). To analyze the contingency table of qualitative data (i.e., actin cage, "Galectin-3 ghost" and actin tail), a Chi2 was performed. $p < 0.05$ was considered as significant: $^{*}p < 0.05$, $^{**}p < 0.01$, $^{***}p < 0.001$, and $^{****}p < 0.0001$.

SUPPLEMENTAL INFORMATION

Supplemental Information includes seven figures, six movies, one table, and Supplemental Experimental Procedures and can be found with this article at http://dx.doi.org/10.1016/j.chom.2014.09.005.

ACKNOWLEDGMENTS

We would like to thank Claude Parsot, Arnaud Echard, and Bruno Goud for tools used in this work. Further, we acknowledge fruitful discussions with all lab members of the DIHP unit, and with Nathalie Sauvonnet and Guy Tran Van Nhieu. Also, we acknowledge Béatrice de Cougny for the design of the graphical abstract and Laurence Langlais for text editing. This work was supported by the Institut Pasteur (PTR 460); by a fellowship from the Fondation pour la Recherche Médicale (FRM) to N.M.; by fellowships from the Pasteur-Weizmann Council, EMBO and the FRM to A.W.; and by a grant from the Region Ile de France to J.E. and G. Tran Van Nhieu (DIM-Malinf). Electron microscopy was performed in the Irving and Cherna Moscowitz Center for Nano and Bio-nano Imaging of the Weizmann Institute. J.E. and S.L.S. are members of the LabEx consortium IBEID. The Imagopole is part of the France-BioImaging infrastructure supported by the French National Research Agency (ANR-10-INSB-04-01, "Investments for the future"). It is further supported by the Conseil de la Region Ile-de-France (Sesame 2007, project Imagopole) and from the FRM (Programme Grands Equipements) (to N.A.). J.E. is supported by an ERC starting grant (Rupteffects, number 261166).

Received: May 2, 2014
Revised: July 21, 2014
Accepted: August 12, 2014
Published: October 8, 2014

REFERENCES

Aickin, M., and Gensler, H. (1996). Adjusting for multiple testing when reporting research results: the Bonferroni vs Holm methods. Am. J. Public Health *86*, 726–728.

Akimana, C., Al-Khodor, S., and Abu Kwaik, Y. (2010). Host factors required for modulation of phagosome biogenesis and proliferation of *Francisella tularensis* within the cytosol. PLoS ONE *5*, e11025.

Blocker, A., Gounon, P., Larquet, E., Niebuhr, K., Cabiaux, V., Parsot, C., and Sansonetti, P. (1999). The tripartite type III secreton of *Shigella flexneri* inserts IpaB and IpaC into host membranes. J. Cell Biol. *147*, 683–693.

Brumell, J.H., and Scidmore, M.A. (2007). Manipulation of rab GTPase function by intracellular bacterial pathogens. Microbiol. Mol. Biol. Rev. *71*, 636–652.

Brumell, J.H., Tang, P., Zaharik, M.L., and Finlay, B.B. (2002). Disruption of the *Salmonella*-containing vacuole leads to increased replication of *Salmonella enterica* serovar typhimurium in the cytosol of epithelial cells. Infect. Immun. *70*, 3264–3270.

Coburn, B., Sekirov, I., and Finlay, B.B. (2007). Type III secretion systems and disease. Clin. Microbiol. Rev. *20*, 535–549.

Dambournet, D., Machicoane, M., Chesneau, L., Sachse, M., Rocancourt, M., El Marjou, A., Formstecher, E., Salomon, R., Goud, B., and Echard, A. (2011). Rab35 GTPase and OCRL phosphatase remodel lipids and F-actin for successful cytokinesis. Nat. Cell Biol. *13*, 981–988.

Davis, M.J., Gregorka, B., Gestwicki, J.E., and Swanson, J.A. (2012). Inducible renitence limits *Listeria monocytogenes* escape from vacuoles in macrophages. J. Immunol. *189*, 4488–4495.

Derré, I., Pypaert, M., Dautry-Varsat, A., and Agaisse, H. (2007). RNAi screen in *Drosophila* cells reveals the involvement of the Tom complex in *Chlamydia* infection. PLoS Pathog. *3*, 1446–1458.

Dickenson, N.E., Choudhari, S.P., Adam, P.R., Kramer, R.M., Joshi, S.B., Middaugh, C.R., Picking, W.L., and Picking, W.D. (2013). Oligomeric states of the *Shigella* translocator protein IpaB provide structural insights into formation of the type III secretion translocon. Protein Sci. *22*, 614–627.

Ehsani, S., Santos, J.C., Rodrigues, C.D., Henriques, R., Audry, L., Zimmer, C., Sansonetti, P., Tran Van Nhieu, G., and Enninga, J. (2012). Hierarchies of host factor dynamics at the entry site of *Shigella flexneri* during host cell invasion. Infect. Immun. *80*, 2548–2557.

Grant, B.D., and Donaldson, J.G. (2009). Pathways and mechanisms of endocytic recycling. Nat. Rev. Mol. Cell Biol. *10*, 597–608.

Håkansson, S., Schesser, K., Persson, C., Galyov, E.E., Rosqvist, R., Homblé, F., and Wolf-Watz, H. (1996). The YopB protein of *Yersinia pseudotuberculosis* is essential for the translocation of Yop effector proteins across the target cell plasma membrane and displays a contact-dependent membrane disrupting activity. EMBO J. *15*, 5812–5823.

Hammond, G.R.V., Dove, S.K., Nicol, A., Pinxteren, J.A., Zicha, D., and Schiavo, G. (2006). Elimination of plasma membrane phosphatidylinositol (4,5)-bisphosphate is required for exocytosis from mast cells. J. Cell Sci. *119*, 2084–2094.

High, N., Mounier, J., Prévost, M.C., and Sansonetti, P.J. (1992). IpaB of *Shigella flexneri* causes entry into epithelial cells and escape from the phagocytic vacuole. EMBO J. *11*, 1991–1999.

Hoffmann, C., Finsel, I., Otto, A., Pfaffinger, G., Rothmeier, E., Hecker, M., Becher, D., and Hilbi, H. (2014). Functional analysis of novel Rab GTPases identified in the proteome of purified *Legionella*-containing vacuoles from macrophages. Cell. Microbiol. *16*, 1034–1052.

Hume, P.J., McGhie, E.J., Hayward, R.D., and Koronakis, V. (2003). The purified *Shigella* IpaB and *Salmonella* SipB translocators share biochemical properties and membrane topology. Mol. Microbiol. *49*, 425–439.

Ingmundson, A., Delprato, A., Lambright, D.G., and Roy, C.R. (2007). *Legionella pneumophila* proteins that regulate Rab1 membrane cycling. Nature *450*, 365–369.

Janmey, P.A., and Kinnunen, P.K.J. (2006). Biophysical properties of lipids and dynamic membranes. Trends Cell Biol. *16*, 538–546.

Janmey, P.A., and Lindberg, U. (2004). Cytoskeletal regulation: rich in lipids. Nat. Rev. Mol. Cell Biol. *5*, 658–666.

Konradt, C., Frigimelica, E., Nothelfer, K., Puhar, A., Salgado-Pabon, W., di Bartolo, V., Scott-Algara, D., Rodrigues, C.D., Sansonetti, P.J., and Phalipon, A. (2011). The *Shigella flexneri* type three secretion system effector IpgD inhibits T cell migration by manipulating host phosphoinositide metabolism. Cell Host Microbe *9*, 263–272.

Kumar, Y., and Valdivia, R.H. (2008). Actin and intermediate filaments stabilize the *Chlamydia trachomatis* vacuole by forming dynamic structural scaffolds. Cell Host Microbe *4*, 159–169.

Mallo, G.V., Espina, M., Smith, A.C., Terebiznik, M.R., Alemán, A., Finlay, B.B., Rameh, L.E., Grinstein, S., and Brumell, J.H. (2008). SopB promotes phosphatidylinositol 3-phosphate formation on *Salmonella* vacuoles by recruiting Rab5 and Vps34. J. Cell Biol. *182*, 741–752.

Méresse, S., Unsworth, K.E., Habermann, A., Griffiths, G., Fang, F., Martínez-Lorenzo, M.J., Waterman, S.R., Gorvel, J.P., and Holden, D.W. (2001). Remodelling of the actin cytoskeleton is essential for replication of intravacuolar *Salmonella*. Cell. Microbiol. *3*, 567–577.

Mounier, J., Popoff, M.R., Enninga, J., Frame, M.C., Sansonetti, P.J., and Van Nhieu, G.T. (2009). The IpaC carboxyterminal effector domain mediates Src-dependent actin polymerization during *Shigella* invasion of epithelial cells. PLoS Pathog. *5*, e1000271.

Mounier, J., Boncompain, G., Senerovic, L., Lagache, T., Chrétien, F., Perez, F., Kolbe, M., Olivo-Marin, J.-C., Sansonetti, P.J., and Sauvonnet, N. (2012). *Shigella* effector IpaB-induced cholesterol relocation disrupts the Golgi complex and recycling network to inhibit host cell secretion. Cell Host Microbe *12*, 381–389.

Mukherjee, K., Parashuraman, S., Raje, M., and Mukhopadhyay, A. (2001). SopE acts as an Rab5-specific nucleotide exchange factor and recruits non-prenylated Rab5 on *Salmonella*-containing phagosomes to promote fusion with early endosomes. J. Biol. Chem. *276*, 23607–23615.

Niebuhr, K., Giuriato, S., Pedron, T., Philpott, D.J., Gaits, F., Sable, J., Sheetz, M.P., Parsot, C., Sansonetti, P.J., and Payrastre, B. (2002). Conversion of PtdIns(4,5)P(2) into PtdIns(5)P by the *S.flexneri* effector IpgD reorganizes host cell morphology. EMBO J. *21*, 5069–5078.

Ohlson, M.B., Fluhr, K., Birmingham, C.L., Brumell, J.H., and Miller, S.I. (2005). SseJ deacylase activity by *Salmonella enterica* serovar Typhimurium promotes virulence in mice. Infect. Immun. *73*, 6249–6259.

Paz, I., Sachse, M., Dupont, N., Mounier, J., Cederfur, C., Enninga, J., Leffler, H., Poirier, F., Prevost, M.-C., Lafont, F., and Sansonetti, P. (2010). Galectin-3, a marker for vacuole lysis by invasive pathogens. Cell. Microbiol. *12*, 530–544.

Pendaries, C., Tronchère, H., Arbibe, L., Mounier, J., Gozani, O., Cantley, L., Fry, M.J., Gaits-Iacovoni, F., Sansonetti, P.J., and Payrastre, B. (2006). PtdIns5P activates the host cell PI3-kinase/Akt pathway during *Shigella flexneri* infection. EMBO J. *25*, 1024–1034.

Puhar, A., Tronchère, H., Payrastre, B., Nhieu, G.T.V., and Sansonetti, P.J. (2013). A *Shigella* effector dampens inflammation by regulating epithelial release of danger signal ATP through production of the lipid mediator PtdIns5P. Immunity *39*, 1121–1131.

Radtke, A.L., Anderson, K.L., Davis, M.J., DiMagno, M.J., Swanson, J.A., and O'Riordan, M.X. (2011). *Listeria monocytogenes* exploits cystic fibrosis transmembrane conductance regulator (CFTR) to escape the phagosome. Proc. Natl. Acad. Sci. USA *108*, 1633–1638.

Ramel, D., Lagarrigue, F., Pons, V., Mounier, J., Dupuis-Coronas, S., Chicanne, G., Sansonetti, P.J., Gaits-Iacovoni, F., Tronchère, H., and Payrastre, B. (2011). *Shigella flexneri* infection generates the lipid PI5P to alter endocytosis and prevent termination of EGFR signaling. Sci. Signal. *4*, ra61.

Ray, K., Marteyn, B., Sansonetti, P.J., and Tang, C.M. (2009). Life on the inside: the intracellular lifestyle of cytosolic bacteria. Nat. Rev. Microbiol. *7*, 333–340.

Ray, K., Bobard, A., Danckaert, A., Paz-Haftel, I., Clair, C., Ehsani, S., Tang, C., Sansonetti, P., Tran, G.V., and Enninga, J. (2010). Tracking the dynamic interplay between bacterial and host factors during pathogen-induced vacuole rupture in real time. Cell. Microbiol. *12*, 545–556.

Rejman Lipinski, A., Heymann, J., Meissner, C., Karlas, A., Brinkmann, V., Meyer, T.F., and Heuer, D. (2009). Rab6 and Rab11 regulate *Chlamydia trachomatis* development and golgin-84-dependent Golgi fragmentation. PLoS Pathog. *5*, e1000615.

Scott, C.C., Dobson, W., Botelho, R.J., Coady-Osberg, N., Chavrier, P., Knecht, D.A., Heath, C., Stahl, P., and Grinstein, S. (2005). Phosphatidylinositol-4,5-bisphosphate hydrolysis directs actin remodeling during phagocytosis. J. Cell Biol. *169*, 139–149.

Senerovic, L., Tsunoda, S.P., Goosmann, C., Brinkmann, V., Zychlinsky, A., Meissner, F., and Kolbe, M. (2012). Spontaneous formation of IpaB ion channels in host cell membranes reveals how *Shigella* induces pyroptosis in macrophages. Cell Death Dis. *3*, e384.

Singh, R., Jamieson, A., and Cresswell, P. (2008). GILT is a critical host factor for *Listeria monocytogenes* infection. Nature *455*, 1244–1247.

Stenmark, H. (2009). Rab GTPases as coordinators of vesicle traffic. Nat. Rev. Mol. Cell Biol. *10*, 513–525.

van der Goot, F.G., Tran van Nhieu, G., Allaoui, A., Sansonetti, P., and Lafont, F. (2004). Rafts can trigger contact-mediated secretion of bacterial effectors via a lipid-based mechanism. J. Biol. Chem. *279*, 47792–47798.

Weber, S.S., Ragaz, C., and Hilbi, H. (2009). Pathogen trafficking pathways and host phosphoinositide metabolism. Mol. Microbiol. *71*, 1341–1352.

Weiner, A., Dahan-Pasternak, N., Shimoni, E., Shinder, V., von Huth, P., Elbaum, M., and Dzikowski, R. (2011). 3D nuclear architecture reveals coupled cell cycle dynamics of chromatin and nuclear pores in the malaria parasite Plasmodium falciparum. Cell. Microbiol. *13*, 967–977.

Welz, T., Wellbourne-Wood, J., and Kerkhoff, E. (2014). Orchestration of cell surface proteins by Rab11. Trends Cell Biol. *24*, 407–415.

Yam, P.T., and Theriot, J.A. (2004). Repeated cycles of rapid actin assembly and disassembly on epithelial cell phagosomes. Mol. Biol. Cell *15*, 5647–5658.